

JGR Atmospheres

RESEARCH ARTICLE

10.1029/2021JD035321

Key Points:

- Temperature diurnal and semidiurnal tides in the summer turbopause region at midlatitude are investigated by the Michelson interferometer for global high-resolution thermospheric imaging (MIGHTI) and a sodium (Na) lidar
- Diurnal and semidiurnal amplitudes reach as large as 19 K in the turbopause region, and are experiencing considerable dissipation
- The diurnal tide in the turbopause region demonstrates evanescent wave feature with an almost constant phase

Correspondence to:




T. Yuan,
titus.yuan@usu.edu

Citation:

Yuan, T., Stevens, M. H., Englert, C. R., & Immel, T. J. (2021). Temperature tides across the mid-latitude summer turbopause measured by a sodium lidar and MIGHTI/ICON. *Journal of Geophysical Research: Atmospheres*, 126, e2021JD035321. <https://doi.org/10.1029/2021JD035321>

Received 8 JUN 2021
Accepted 6 AUG 2021

Temperature Tides Across the Mid-Latitude Summer Turbopause Measured by a Sodium Lidar and MIGHTI/ICON

T. Yuan¹ , M. H. Stevens² , C. R. Englert² , and T. J. Immel³

¹Center for Atmospheric and Space Sciences, Utah State University, Logan, UT, USA, ²Space Science Division, Naval Research Laboratory, Washington, DC, USA, ³Space Sciences Laboratory, University of California, Berkeley, CA, USA

Abstract Local full diurnal coverage of temperature variations across the turbopause (~90–115 km altitude) is achieved by combining the nocturnal observations of a Sodium (Na) Doppler lidar on the Utah State University (USU) campus (41.7°N, 248.2°E) and NASA Michelson interferometer for global high-resolution thermospheric imaging (MIGHTI)/Ionospheric connection explorer (ICON) daytime observations made in the same vicinity. In this study, utilizing this hybrid data set during summer 2020 between June 12th and July 15th, we retrieve the temperature signatures of diurnal and semidiurnal tides in this region. The tidal amplitudes of both components have similar vertical variation with increasing altitude: less than 5 K below ~98 km but increase considerably above, up to 19 K near 104 km. Both experience significant dissipation near turbopause altitudes, down to ~12 K up to 113 km for the diurnal tide and ~13 K for the semidiurnal tide near 110 km. In addition, while the semidiurnal tidal behavior is consistent with the theoretical predictions, the diurnal amplitude is considerably larger than what is expected in the turbopause region. The tidal phase profile shows a dominance of tidal components with a long vertical wavelength (longer than 40 km) for the semidiurnal tide. On the other hand, the diurnal tide demonstrates close to an evanescent wave behavior in the turbopause region, which is absent in the model results and Thermosphere ionosphere mesosphere energetics and dynamics (TIMED)/Sounding of the atmosphere using broadband radiometry (SABER) observations.

Plain Language Summary Solar thermal tidal wave in the atmosphere is one of the most dominant dynamic features in the upper atmosphere. In this paper, we utilize the temperature results from the recently launched NASA Ionospheric connection explorer (ICON) satellite daytime observation and those by a ground-based Na lidar nighttime measurements in summer 2020 to accomplish 24-h coverage of temperature variations in the upper atmosphere between ~90 and 115 km. This allows us to investigate the tidal wave behavior in one of the least studied upper atmosphere region near 110 km altitude, so called “turbopause” region, above middle latitude in Northern America. The study reveals highly complex diurnal tidal wave features in this region, while the semidiurnal tide is less affected except some wave dissipation.

1. Introduction

Solar thermal tides, generated in the troposphere and stratosphere by absorption of solar radiation and latent heat released due to raindrop formation, are one of the most important sources of dynamical forcing in the mesosphere and lower thermosphere (MLT; Hagan & Forbes, 2002, 2003). Tides propagate zonally, upward and are very sensitive to atmospheric mean-flow (Baumgarten & Stober, 2019; Becker, 2017; McLandress, 2002) that is, closely associated with strong tidal variabilities of various temporal and spatial scales, such as short-term day-to-day variability and interannual variations (Dhadly et al., 2018; She et al., 2004). They modulate the temperature and wind field of the upper atmosphere with considerable amplitude, and affect small-scale dynamical processes through their introduction of large horizontal and vertical gradients in both wind and temperature (Becker, 2017; Cai et al., 2014; Liu & Hagan, 1998; Yuan et al., 2014). Considerable progress has been made in understanding tidal wave dynamics over the past few decades through theoretical and experimental investigations (Forbes et al., 2008; Oberheide et al., 2011; Yuan, Schmidt, et al., 2008; Yuan et al., 2006, 2010). However, the tidal behaviors above ~100 km and across the turbopause area, where the dominant mixing mechanism in the atmosphere transitions from eddy mixing

to molecular diffusion, are difficult to measure, mostly due to the lack of regionally distributed, high precision experimental data. Increased measurement capability in this region, where viscous tidal dissipation is hypothesized (Forbes & Garrett, 1979), is critical for understanding tidal wave upward propagation into the middle and upper thermosphere and various ion-neutral coupling processes, such as the formation of middle latitudes sporadic-E layers (Cai et al., 2017; Carter & Forbes, 1999). While the tidal wave signatures in this region have been investigated and discussed using sounding of the atmosphere using broadband radiometry (SABER) observations (Forbes et al., 2008; Zhang et al., 2006), a broad window, at least 60-days wide, has to be implemented to achieve 24-h coverage across all longitudes. This relatively long sampling window algorithm cannot resolve tidal wave variability at high spatial and temporal resolution, essentially the detailed changes of tidal wave behavior as they pass through this highly variable region.

The advanced USU Na Doppler lidar (41.7°N, 248.2°E) has the capability of measuring temperature and winds in the mesopause region (~80–105 km), covering the full diurnal cycle through measuring the thermal broadening and Doppler shift of the laser-induced fluorescence spectrum of mesospheric Na atoms (Krueger et al., 2015). Its multi-year observations have been utilized to establish the tidal climatology at middle latitudes of North America (Yuan, Schmidt, et al., 2008; Yuan et al., 2010; 2014). As a single point observation, these lidar-measured tidal wave signatures are the combination of migrating (sun-synchronous) and non-migrating (not sun-synchronous) tides. While the standard Na lidar nighttime capability allows high-quality measurements up to ~105 km, its daytime observations are limited to near or below 100 km for most of the year. This is because of large daytime sky background noise, especially during the summer when the maximum solar elevation angle can be more than 70° near the location of the lidar station. Furthermore, the mesospheric Na abundance, which the Na lidar measurement relies upon, is close to its annual minimum in the summertime (Yuan et al., 2012). These lead to the lidar daytime measurements in the summer can only reach as high as ~98 km due primarily to these daytime limitations. Recent upgrades of the system, especially the installation of a ~5 m² receiving mirror, have enabled nocturnal lidar measurements up to ~115 km. However, daytime observations near and above 100 km are still quite challenging and not available at all for the summer 2020 campaign.

The Michelson Interferometer for Global High-resolution Thermospheric Imaging (MIGHTI) onboard the NASA Ionospheric Connection Explorer (ICON) satellite, launched in October 2019, measures neutral temperature by imaging the molecular oxygen atmospheric band (A-band) day and night (Englert et al., 2017; Immel et al., 2018; Stevens et al., 2018). Temperature is inferred by measuring the relative intensity of the A-band emission in three discrete wavelength channels as well as two background channels on either side of the band. The A-band emission rates vary from night to day, providing a target in nighttime observations between ~90 and 105 km and daytime A-Band observations up to ~140 km and, and in the currently released data version, retrieved temperatures up to 115 km. With a 27° inclination orbit, MIGHTI/ICON can provide day-night coverage between ~90 and 105 km within the latitude range between 12°S and 42°N for tidal wave investigations over the diurnal cycle within 27 days (Forbes et al., 2017) with a gap in longitudinal coverage in the Southern Atlantic Anomaly (SAA). However, the tidal activities in the turbopause region cannot be investigated by MIGHTI/ICON alone, due to the limited vertical extent of its nighttime measurements (~105 km).

In this paper, we combine the high quality nocturnal USU Na lidar and the nearby daytime MIGHTI/ICON observations between June 12 and July 15, 2020 to achieve a full set of diurnal cycle temperature measurements in the lower thermosphere, ~90–115 km, above the USU location. In this study, to estimate any potential bias between the two instruments, the nighttime temperatures are directly compared between the two datasets at altitudes where they overlap (90–105 km), while the daytime MIGHTI temperatures are compared with a multi-year lidar climatology and the observations during a USU Na lidar campaign in March 2021 (Appendix). The diurnal and semidiurnal tidal temperature amplitude and phase profiles from the upper mesosphere to the lower thermosphere across the turbopause (~110 km) are derived from this hybrid data set. A tidal climatology based on the lidar observations between 2002 and 2008 (Yuan et al., 2010), when the system was operating at Colorado State University (CSU; 41°N, 255°E) to serve as a reference. The data involved in this study are described in Section 2; the derived tidal results are presented in Section 3, followed by the discussion of the results in Section 4. A summary of this investigation is provided in Section 5.

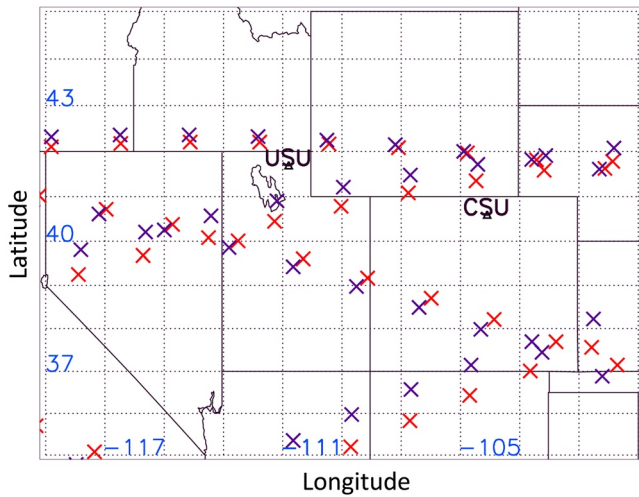


Figure 1. Michelson interferometer for global high-resolution thermospheric imaging (MIGHTI)/Ionospheric connection explorer (ICON) observations (red crosses for MIGHTI-A; purple crosses for MIGHTI-B) near 100 km altitude on June 20, 2020 in the vicinity of the Utah State University (USU) sodium (Na) lidar station (35°N–42°N and 120°W–00°W).

2. Data and Models Involved

The lidar operated 16 nights across the summer solstice between June 12 and July 15, 2020, while we include 20 days of overlapping MIGHTI/ICON data from both MIGHTI sensors (MIGHTI-A and MIGHTI-B that are pointing at two perpendicular directions) during the period of this study. The version 4 (v04) MIGHTI-A daytime data are assembled from ~90 to 115 km while the v04 MIGHTI-B daytime data are assembled from ~99 to 115 km. These multi-day hourly averaged lidar temperature profiles with 2-km vertical resolution are binned in one-hour local time bins between 20:00 and 04:00, establishing the average temperature variation during summer nights. To match the MIGHTI vertical resolution (~3-km), the lidar temperature profiles are further smoothed with a 3-km boxcar window. The uncertainty of the lidar measurements is dominated by photon shot noise (the lidar accuracy is better than 0.1 K; Krueger et al., 2015). Due to decreasing Na number densities above 100 km, the hourly temperature uncertainty (statistical uncertainty), which is less than 0.5 K near 95 km and around 1 K at 100 km, increases quickly with increasing altitude. For example, around 110 km, the averaged uncertainty of single hourly profile reaches ~15 K. Here, the upper limit of the lidar temperature uncertainty is set to 30 K (any temperatures with uncertainties larger than 30 K are neglected). This is slightly above the hourly uncertainty near 115 km under a normal condition where the temperature is near or above 300 K. Because the lidar has 14–16 hourly profiles for each LST during this period, the final uncertainties are about one quarter of those for the single hourly lidar measurements.

Meanwhile, MIGHTI/ICON observations between 35°N–42°N latitude and 240°E–260°E longitude are chosen and binned hourly to establish the averaged daytime temperature variations. Figure 1 illustrates the MIGHTI/ICON measurements within this geographic grid near 100 km, including both MIGHTI-A and MIGHTI-B, on the day of the summer solstice (June 20, 2020) within this region, showing the good overlap between the two instruments. The figure also demonstrates the geographic distance between the two lidar stations, which is relatively small from the large geophysical scale perspective, allowing us to utilize the tidal climatological results obtained at CSU. A relatively detailed discussion on the continuity of the two lidar datasets is presented in Yuan et al., (2019). Table 1 lists the number of MIGHTI and the lidar hourly temperature profiles for each local solar time near the USU Na lidar station during this period (For example, LST 12 represents the period between LST 12:00 and 13:00). Notice that the number of MIGHTI profiles during the daytime is considerably higher than that during the nighttime hours (shaded cells), except in the late afternoon, showing good daytime coverage by MIGHTI. This is because the cadence of the MIGHTI measurements is twice as long during the night (60 s) compared to the day (30 s). The measurement precision is 1 K between 90 and 105 km during the day whereas, during the night, it increases from 1 K at 90 km to 3 K at 105 km. The accuracy is estimated to be ~12 K for both nighttime and daytime MIGHTI/ICON temperature measurements for the version 04 data used here, and that accuracy is

separately applied to each mode of operation so that, for example, it can be positive for all nighttime data and negative for all daytime data. Both the lidar and MIGHTI data are then interpolated onto the same 3-km altitude grid, between 85 and 115 km.

Figure 2 shows the comparisons of the daytime and nighttime temperature measurements between the two instruments in the MLT region from 85 km to 115 km. Note that, for the daytime temperature comparison with MIGHTI/ICON, we introduce multi-year, daytime lidar observations during the same day-of-year period between 2012 and 2016 as the established climatological daytime temperatures. This is because the lidar was not set up to run daytime-operations during summer 2020. For the comparison in Figure 2, the local solar times were chosen between 23:00 and 01:00 for nighttime and 13:00–15:00 for daytime. The nighttime

Table 1
Number of MIGHTI (Lidar) Profiles for Each Local Solar Time

LST	00:00	01:00	02:00	03:00	04:00	05:00	06:00	07:00
Profiles	3(16)	5(16)	7(16)	2(16)	3/(14)	10	14	16
LST	08:00	09:00	10:00	11:00	12:00	13:00	14:00	15:00
Profiles	16	16	18	20	18	16	17	12
LST	16:00	17:00	18:00	19:00	20:00	21:00	22:00	23:00
Profiles	8	6	4	4	1(15)	1(16)	3(16)	3(16)

Abbreviation: MIGHTI, Michelson interferometer for global high-resolution thermospheric imaging.

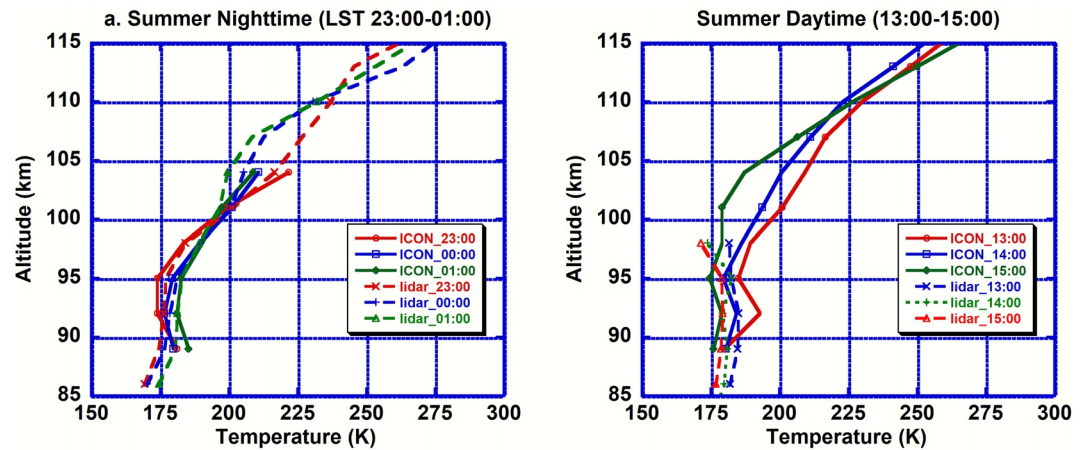


Figure 2. Temperature comparisons between Utah State University (USU) sodium (Na) lidar (dashed lines) and Michelson interferometer for global high-resolution thermospheric imaging (MIGHTI)/Ionospheric connection explorer (ICON; solid) during daytime (left plot) for local solar time: 13:00 (green), 14:00 (blue), 15:00 (red); and nighttime (right plot) for local time: 23:00 (red), 00:00 (blue), and 01:00 (green). The MIGHTI accuracy is ~ 12 K for daytime and nighttime.

temperature comparison shows excellent agreement between the observations of the two instruments below 100 km, while the difference increases slightly above. Near 104 km, the MIGHTI nighttime temperature observations for these hours are ~ 4 K higher than the corresponding lidar temperature observations, which is within the magnitude of the nighttime statistical uncertainty at this altitude. These MIGHTI nighttime averages only include data from MIGHTI-A, since there is no MIGHTI-B data below 100 km in version 04. The daytime temperature measurements by the two instruments also demonstrate very good agreement in the overlapping altitude range, and the differences are within the MIGHTI daytime accuracy (~ 12 K). Further daytime temperature comparisons have been conducted in March 2021 that confirm the consistency between the two instruments (see [Appendix](#)). As the figure shows, the lidar can only reach ~ 98 km in the daytime with the uncertainty that is, one order of magnitude higher than that of the nighttime observations because of those aforementioned limitations. The figure also illustrates a common summertime temperature feature: it changes slowly around 180 K between 85 and 100 km, but increases quickly above ~ 105 km when reaching the thermosphere. To further estimate the potential bias between the two sets of temperature measurements, we plot the averaged lidar and MIGHTI temperature variations at 99 km in a 24-h period in [Figure 3](#), along with the reconstructed tidal variation that is, discussed in [Section 3](#). During the nighttime (LST 20:00–04:00), the lidar temperatures and the concurrent MIGHTI temperatures are highly correlated and demonstrate the same dynamic variation. The diurnal and semidiurnal cycles, utilized to reconstruct the temperature variation at 99 km, are also presented in this figure, which indicates the two major tidal components are relatively in phase with each other in the morning hours.

Given the agreements of the two data sets discussed above, we conclude that it is possible to combine the two temperature observations around the USU location to achieve continuous 24-h daytime and nighttime temperature coverage in the MLT. Furthermore, these comparisons demonstrate that the two sets of temperatures are uniquely complementary: The Na lidar has high-quality measurements during the night up to 115 km, while MIGHTI provides the daytime temperature up to a similar altitude (~ 113 km in this data set). Since the potential bias between the two measurements is within their uncertainties, by combining the hourly temperature profiles of the lidar nighttime observations and the local MIGHTI daytime observations, high-quality full diurnal cycle coverage in the MLT up to ~ 115 km can be achieved. It is worth noting that, for this altitude region, this is not feasible for either instrument. For this study, the MIGHTI temperature range is expanded slightly to 85–115 km utilizing the cubic spline extrapolation. The data between ~ 90 and 113 km are utilized for the tidal wave investigations.

Based on this unique full diurnal cycle data set, a linear least squares fitting algorithm that includes diurnal (24-h), semidiurnal (12-h), terdiurnal (8-h), and quardiurnal (6-h) components is applied to the temperature

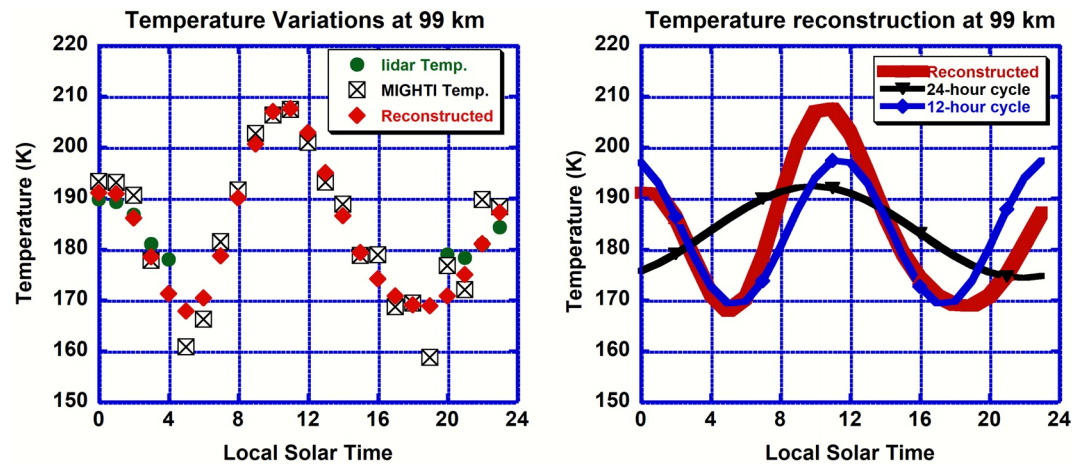


Figure 3. Averaged temperature variations near 99 km in summertime (top) observed by the Na lidar (solid dots) and Ionospheric connection explorer (ICON)/Michelson interferometer for global high-resolution thermospheric imaging (MIGHTI; squares filled with cross), along with the tidal reconstructed temperature variation (red diamonds). (bottom) The diurnal (black) and semidiurnal (blue) cycles are utilized to reconstruct the temperature variation at 99 km. The MIGHTI accuracy is ~ 12 K for daytime and nighttime.

variation at each altitude to retrieve the tidal amplitude and phase profiles, as shown in Equation 1, along with the associated fitting uncertainties.

$$T_0 = \bar{T} + \sum_{i=1}^4 A_i \cos\left(\frac{2\pi i}{24}t - \phi_i\right), \quad (1)$$

where \bar{T} is the mean temperature, ..., $i = 1, 2, 3$, and 4 for diurnal, semidiurnal, terdiurnal, and quadriurnal tides, respectively. A_i and ϕ_i represents the tidal amplitude and phase respectively for the i th tidal component. Here, only the dominant diurnal and semidiurnal tidal components are presented, since terdiurnal and quadriurnal tidal components are usually much less significant and inconsistent compared to the former two tidal components. Figure 5 illustrates both the tidal amplitude and tidal phase profiles for these two important tidal components. For reference, the tidal results from the multi-year Na lidar climatology are obtained at CSU and the CTMT predictions based on the Hough Mode Extension (HME; Oberheide et al., 2011) are also presented in the figure. As we mentioned earlier, the CTMT results are calculated and constrained by the global tidal measurements from SABER and TIDI on board the TIMED satellite, which is required to use a minimum of 60 days of observations.

The combined temperature data are shown in the top contour plot in Figure 4, where the nighttime data (from 20:00 to 04:00 LST) are using the lidar temperatures and the daytime data (from 05:00 to 19:00 LST) are filled with MIGHTI measurements. Data near the terminator (90° – 105° Solar Zenith Angle) are removed from the MIGHTI pipeline due to the rapidly changing lighting conditions along the line of sight which compromises the temperature retrieval. For the lidar observation, although the sky becomes relatively dark after 20:00 LST, the lower thermosphere is still illuminated during the early evening, causing high background noise and, thus, increasing the measurement uncertainty in this region. Linear extrapolation is applied to the lidar profile at this hour (20:00 LST) to retrieve the temperatures at 113 km. Overall, the figure shows the potential biases between the two instruments during summer 2020 are insignificant, compared with geophysical variations, and this hybrid data set shows good continuity of temperature variations with clear tidal signatures.

To facilitate this study with theoretical values, the Hamburg Model of the Neutral and Ionized Atmosphere (HAMMONIA) and the Climatological Tidal Model of the Thermosphere (CTMT) are introduced to serve as the references for mean temperature and tides in the turbopause region, respectively (see brief descriptions below). Previous collaborative studies between the lidar and the two models (Yuan, Schmidt, et al., 2008; Yuan, She, et al., 2008; Yuan et al., 2014) have shown the models' relatively realistic predictions of both the mean-field climatology and its tidal components. In this investigation, we

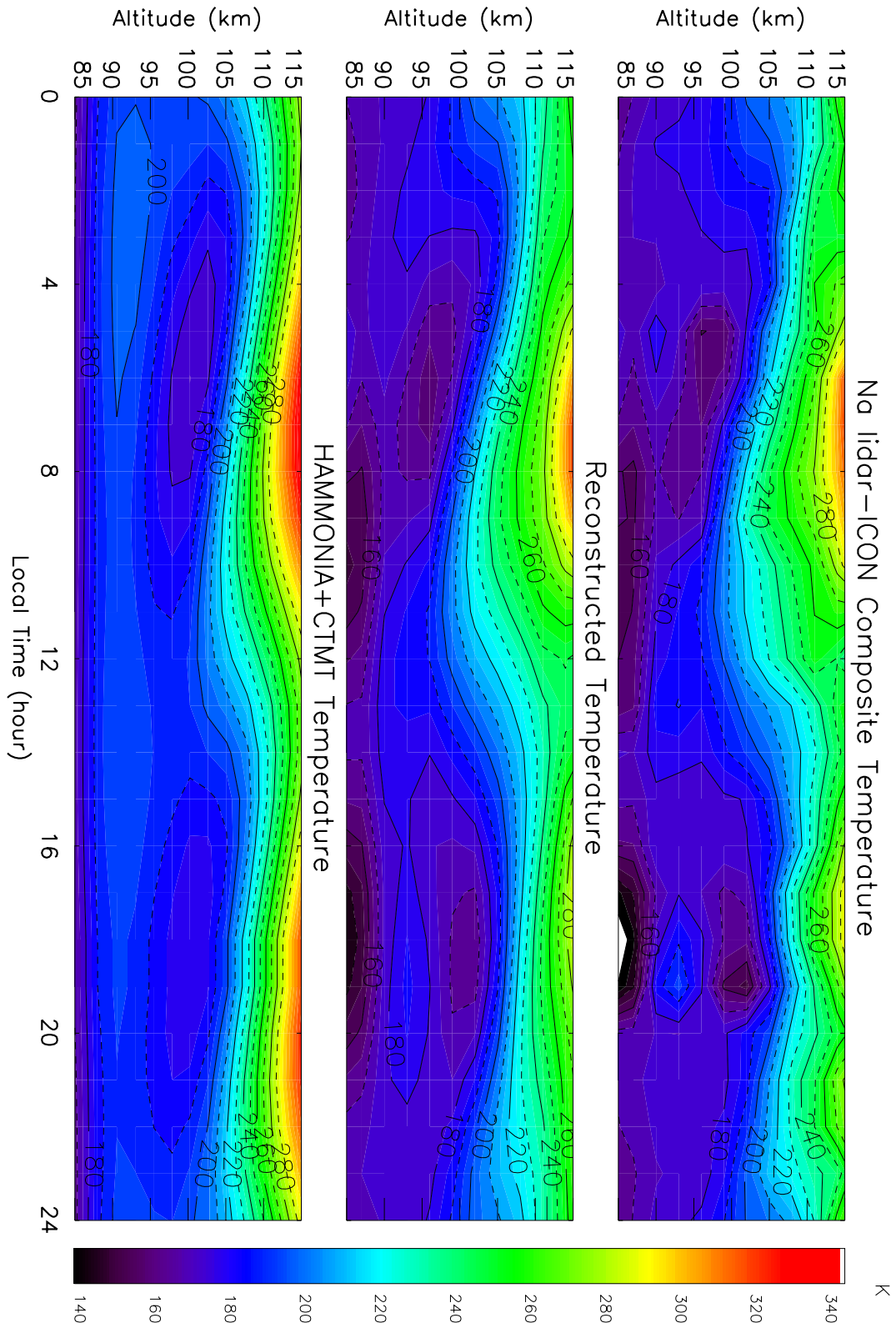


Figure 4.

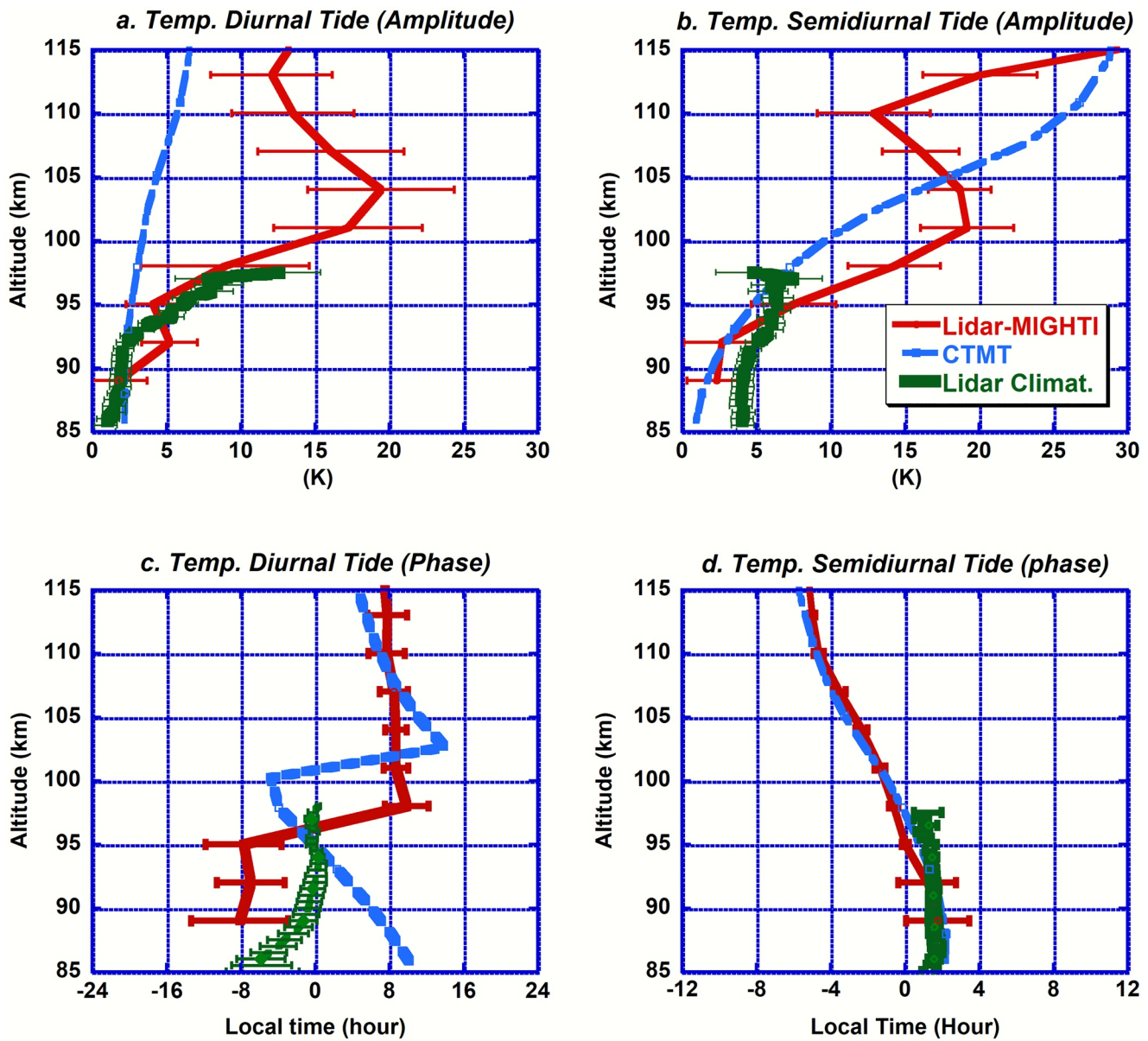


Figure 5. Temperature diurnal (left column) and semidiurnal (right column) amplitude (top row) and phase profiles (bottom row) derived from the new lidar-Michelson interferometer for global high-resolution thermospheric imaging (MIGHTI) observation (red-solid), the multi-year lidar climatology (green solid) and climatological tidal model of the thermosphere (CTMT) output near Utah State University (USU) location (blue dashed line).

add the CTMT tidal outputs (two cosine functions with CTMT diurnal tidal amplitudes and phases: $T_{\text{mean}} + A_{24} \cos\left(\left(2\pi / 24\right)t + \phi_{24}\right) + A_{12} \cos\left(\left(2\pi / 12\right)t + \phi_{12}\right)$, A_{24} , A_{12} are CTMT diurnal and semidiurnal amplitudes; ϕ_{24} , ϕ_{12} are CTMT diurnal and semidiurnal phase) on top of the HAMMONIA monthly mean temperature field, T_{mean} , to simulate the temperature variations across the turbopause region above USU location.

Figure 4. Summertime temperature variations over local times established through the combination of the Utah State University (USU) sodium (Na) lidar nocturnal observations and nearby Michelson interferometer for global high-resolution thermospheric imaging (MIGHTI)/Ionospheric connection explorer (ICON) daytime measurements (top), the reconstructed temperature variations based on the tidal fitting parameters (middle) and the theoretical results based on hybrid data product between Hamburg model of the neutral and ionized atmosphere (HAMMONIA) and climatological tidal model of the thermosphere (CTMT).

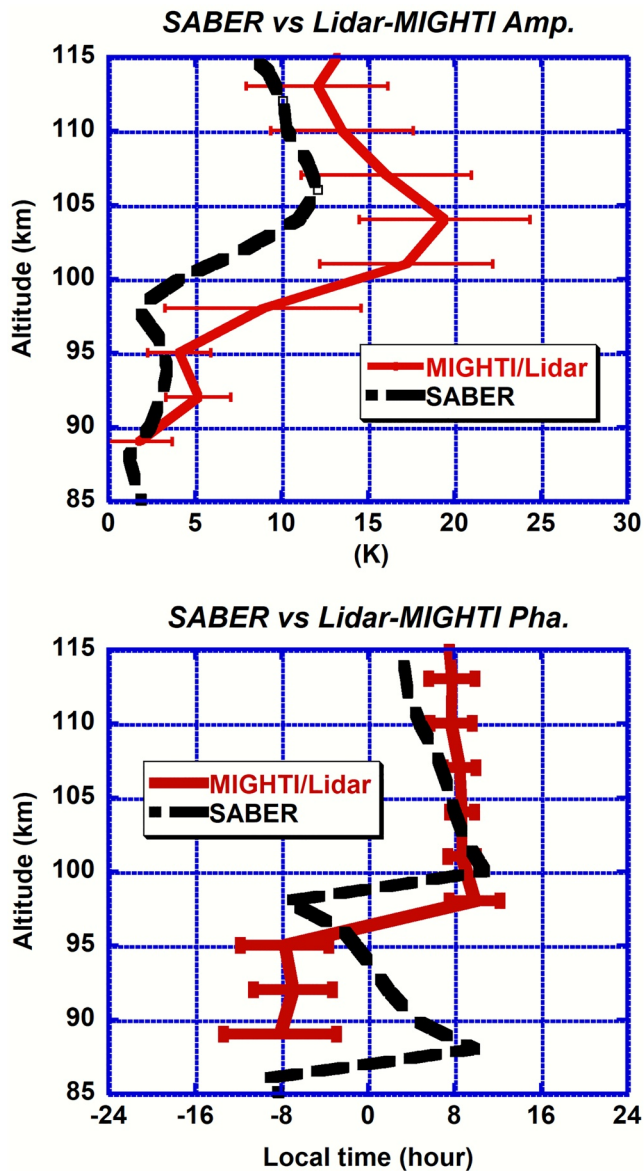


Figure 6. Diurnal tidal amplitude (top) and phase (bottom) comparisons between the new lidar-Michelson interferometer for global high-resolution thermospheric imaging (MIGHTI) measurements and Thermosphere ionosphere mesosphere energetics and dynamics (TIMED)/Sounding of the atmosphere using broadband radiometry (SABER) observations near Utah State University (USU) location between 2002 and 2008.

duced by the MIGHTI accuracy ($\sim 3\text{--}6$ K for tidal amplitude and less than 4 h for tidal phase) are also estimated by calculating differences between the two sets of tidal results when the MIGHTI daytime temperatures are increased and decreased by 12 K. The uncertainties in the figure include both the fitting uncertainties and the uncertainties due to the MIGHTI accuracy by adding the two in quadrature. While the semidiurnal tidal amplitude is similar to the model prediction (except for the dissipation near 110 km), the newly observed diurnal amplitude is considerably larger than the CTMT results above 95 km, which have peaked near 115 km with less than 7 K. Because of this large discrepancy, the archived SABER diurnal tidal amplitude and phase profiles near USU location (Yuan et al., 2010) based on its observation between 2002 and 2008 are introduced in Figure 6 (For the detailed description of

HAMMONIA is a chemistry climate model (CCM) that extends from the surface to the thermosphere, up to about 250 km. As described by Schmidt et al. (2006), it combines physics from the European Center Hamburg Model 5/Middle Atmosphere European Center Hamburg Model 5 (ECHAM5/MAECHAM5) general circulation model (Roegner et al., 2006) and the Model for Ozone And Related chemical Tracers (MOZART3) chemistry scheme, along with several parameterizations to account for important processes in the upper atmosphere. Gravity waves (GW) are parameterized and launched at 700 hPa (about 3 km), using a method proposed by Hines (1997a, 1997b) for waves of non-orographic origin. The planetary wave effect in HAMONNIA comes from self-consistently generated lower-atmosphere dynamics down to the Earth's surface. The monthly mean climatological temperature near the summer solstice in the MLT presented here is obtained from a 35-years simulation (1985–2019) for the appropriate solar minimum conditions.

The Climatological Tidal Model of the Thermosphere (CTMT) is a physics-based empirical tidal model of the thermosphere. It utilizes observed tidal temperatures and winds from the Thermosphere Ionosphere Mesosphere Energetics and Dynamics (TIMED) satellite in the mesosphere and lower thermosphere region to constrain a linear tidal model for the thermosphere. See Oberheide and Forbes (2008) and Oberheide et al. (2011) for details and model validation. Although CTMT, as a data-driven model, produces relatively realistic tidal fields in the zonal wind (u), meridional wind (v), vertical wind (w), temperature (T), and neutral density (ρ) throughout the thermosphere, it has to be pointed out that the model inherently tends to underestimate tidal amplitudes observed at a single ground-based station (Yuan et al., 2014). This is because more smoothing in time and space is needed to perform the underlying tidal temperature and wind diagnostics of the TIMED satellite data.

3. Tidal Results

The tidal amplitudes profiles for both diurnal and semidiurnal tide are quite similar: they are small below 95 km (less than 5 K), which is consistent with early tidal climatology (Yuan, Schmidt, et al., 2008; Yuan et al., 2010), but increase quickly going to higher altitudes, reaching a peak of ~ 19 K near the altitude of 104 km. Then the amplitudes start to decrease as the tides propagate into the turbopause region, most likely due to dissipation. The diurnal tide drops to ~ 12 K near 113 km, while the semidiurnal tidal amplitude decreases to ~ 13 K at 110 km, before it increases dramatically above. In addition to the fitting uncertainty (~ 3 K for tidal amplitude and less than 2 h for tidal phase), those in-

SABER tidal algorithm, see Zhang et al., 2006). Indeed, although the SABER tidal amplitude is larger than the CTMT results, it is still considerably less than the new tidal results between ~ 95 and 105 km, with its maximum ~ 12 K near 106 km. Above 110 km, the differences are close to the fitting uncertainty. The SABER observations also identified the tidal dissipation zone above 105 km, similar to our new observations.

The newly measured summertime diurnal tidal phase profile in turbopause region also demonstrates a quite distinct feature compared with the model results in Figure 5c and TIMED/SABER measurements in Figure 6 in the vicinity of USU/CSU. As expected, the CTMT and the SABER tidal phase results are quite similar. They indicate the typically consistent downward phase progression (upward wave propagation) with a vertical wavelength ~ 20 km below 100 and ~ 40 km between 100 and 115 km, based on their vertical phase velocities. However, the newly observed diurnal tidal phase shows the almost constant phase value above 100 km, which implicates a likely “evanescent” wave behavior or a propagating tide with a very long vertical wavelength. Due to limited altitude range of the observations, it is difficult to calculate the summertime diurnal tide vertical wavelength. The new phase profile below 98 km is fairly similar to the established tidal climatology (Yuan et al., 2010), except for a roughly 8-h shift. The considerable phase shift occurs near 100 km in the CTMT results and the SABER observations, which also appears in the new diurnal phase profile at 95 km. On the other hand, the new semidiurnal tidal phase profile demonstrates a robust upward propagating semidiurnal tide with a consistent vertical wavelength longer than 40 km, in excellent agreement with the CTMT results.

Utilizing these tidal results and following Equation 1, we reconstruct the temperature variation between 85 and 115 km, as shown in the middle contour plot in Figure 4. The reconstructed temperature variation matches the experimental observations very well, demonstrating the fidelity of the fitting. It captures the major variations and demonstrates the reliability of these tidal results. For example, the reconstructed temperatures below 100 km are mostly near and below 200 K with relatively small vertical gradients, which is consistent with the observations. The two observed cold areas (one occurs in the early morning near 95 km, the other occurs in the later afternoon around 100 km) also appear in the reconstructed temperature. Above 100 km within the turbopause region, however, both temperatures increase quickly, approaching ~ 300 K near 115 km. There is a significant temperature modulation between 100 and 115 km occurring in the morning hours. Its maximum (~ 310 K) first appears at 115 km near $06:00$ a.m. and slowly progresses downward at a later time. At noon, its peaks slightly below 100 km. Its vertical phase speed agrees with that of the semidiurnal tide, implying it is dominated by the semidiurnal tide. A secondary maximum occurs in the local afternoon in the turbopause region with a peak value of ~ 290 at 115 km.

4. Discussion

Facilitated by CTMT, a previous study on vertical tidal wind (Yuan et al., 2014) suggested that migrating tides contribute mostly to the tidal modulations in the MLT above the mid-latitudes of Northern America, and the diurnal tide has its annual minimum amplitude around the summer solstice. Since the vertical wind component and temperature component of the tide are closely related through adiabatic processes (She et al., 2016), it is appropriate to assume that, climatologically, the temperature tidal component follows the vertical wind component.

This work shows a distinct diurnal tidal phase feature in the upper mesosphere and into the turbopause region, which implicates very different tidal behaviors in these two parts of the upper atmosphere. Such disparate tidal behaviors can be the indication of the dominance of different diurnal tidal components in different altitude ranges of the MLT. For example, the major non-migrating component, diurnal eastward wavenumber 3 (DE3), has a vertical wavelength of over 50 km, while that of the dominant migrating diurnal westward wavenumber 1 (DW1) is around 20 km most of the time. Because the upward propagation of tides is sensitive to the mean-flow, the migrating diurnal tide with relatively slow vertical phase speed can be easily dissipated. The DE3 component with much faster vertical phase speed, on the other hand, can reach much higher altitudes into the ionosphere E region. As the zonal mean flow changes direction, from eastward to westward, between ~ 100 and 120 km during summer, the change

in this tidal feature can be expected. Furthermore, the DE3 component also peaks during the summertime, inducing large diurnal temperature modulation. On the other hand, it is believed that DE3 mostly affects the upper atmosphere of equatorial and low latitude (Hagan & Forbes, 2002), and contributes insignificantly to the mid-latitude MLT. The almost constant diurnal tidal phase profile, coupled with the decaying amplitude above ~ 100 km, also fits the description of an “evanescent” wave behavior belongs to a diurnal trap mode. When studying the effects of changing atmospheric dissipation on the migrating diurnal tide in the MLT, Forbes and Hagan (1988) found that it's broadening to higher latitude during the solstice when the dominant Hough mode (1, 1) couples into the first symmetric and asymmetric evanescent Hough modes (1, -2) and (1, -1), increasing the total vertical wavelength. Yuan, Schmidt, et al. (2008) suggested the mean-flow variation could switch the tidal behavior from propagating to evanescent by changing the vertical wavenumber square of the tide, when the equivalent depth (eigenvalue of the solution of Laplace tidal equation) becomes negative (Forbes, 1995). In addition, GW have some significant impact on tidal propagation and vice versa (Becker, 2017; Ortland & Alexander, 2006). For example, GW drag can also alter the tidal phases and vertical wavelength, while the observed tidal amplitude dissipation could be due to GW-induced turbulence vertical diffusion. Since the turbopause region overlaps with the dynamo region, ion-drag effects on the damping of the tidal amplitude also need to be considered. However, the detailed dynamic mechanism underlying this unique diurnal tidal behavior is out of the scope of this study, because it involves complex, high-resolution global scale numerical simulation to produce the variations of each tidal mode in this region. Meanwhile, the semidiurnal tide in the turbopause region appears to be dominated by the migrating tidal component with typical long vertical wavelength (see Figure 5d). Intriguingly, an abrupt $\sim 180^\circ$ phase shift relative to the one below 105 km occurs.

The bottom contour plot in Figure 4 illustrates the theoretical temperature variation between 85 and 115 km above the USU location based on the hybrid product of HAMMONA and CTMT, as we discussed earlier. The predictions are in good agreement with the reconstructed temperature variation (middle contour plot in Figure 4), including the local time of temperature maxima and minima. Similar to the observation, the temperature maximum occurs in the early morning and late afternoon hours in turbopause region, along with two temperature minima near 100 km (one in the early morning, the other with slightly higher temperature in the late afternoon and early evening). One major difference is the magnitude of the two maxima/minima. In the numerical results, they are of a similar magnitude, while the observations clearly indicate the dominance of the early morning maximum and minimum. This is due to the considerably smaller diurnal tidal amplitude in CTMT, as shown in Figure 5, compared with the new experimental results. Combined with the large semidiurnal tidal amplitude in the model, this results in the dominance of the 12-h modulation in the turbopause region in the numerical simulation. The observation, by contrast, show similar amplitude values for both diurnal and semidiurnal tides, which leads to an apparent 24-h modulation with the dominance of the morning maximum when the diurnal crest is superimposed on the first semidiurnal crest.

As we mentioned earlier, the oversampling and smoothing of the experimental data (SABER) in CTMT can lead to the underestimation of tidal amplitude. However, the semidiurnal tide does not seem to be affected, as it agrees with the observed tide reasonably well except for the tidal dissipation. The unexpected large diurnal tidal amplitude, along with its almost constant phase in the turbopause region, indicates the diurnal tidal behaviors in this region is far from understood.

5. Summary and Conclusions

The turbopause region is one of the least explored upper atmosphere section, but plays a critical role in wave propagation into the thermosphere and various ion-neutral coupling processes. The understanding of its dynamic and thermal features, especially the tidal wave behaviors there, is thus highly important. In this study, by taking advantage of high cadence MIGHTI temperature observations and the significantly improved USU Na lidar data, we combine 16-nights of the lidar nocturnal observations at USU with 20 days of MIGHTI/ICON daytime measurements nearby in summer 2020. This unique hybrid data set achieves high-quality full diurnal cycle temperature coverage from the upper mesosphere across the

turbopause region, up to 115 km, which cannot be accomplished by either instrument alone. It enables us to retrieve the local temperature diurnal and semidiurnal tidal amplitudes and phases in this region. While these tides in the upper mesosphere below 98 km are fairly consistent with the established tidal climatology, several new findings in the summer turbopause region above mid-latitude are investigated in this paper.

1. Both diurnal and semidiurnal tidal amplitudes increase quickly above 100 km with increasing altitude, as large as ~ 19 K near 104 km, considerably larger than their values below (less than 6 K). They all likely experience dissipation near 104 km, but the semidiurnal tide recovers quickly above 110 km, while the diurnal tidal amplitude keeps decreasing, down to ~ 12 K near 113 km.
2. The newly observed diurnal tide in the turbopause region is considerably stronger ($>50\%$) than the model prediction and the TIMED/SABER observations with a very different tidal phase profile. Its amplitude is in a similar magnitude of the semidiurnal tide, while the model predicts the complete dominance of the latter. In the turbopause region, this leads to a dominant maximum in the morning hours in the observations, instead of a double-peak feature in the model results.
3. While the semidiurnal tidal phase profile indicates a typical upward propagating tidal wave behavior with a vertical wavelength longer than 40 km, the diurnal tidal behavior in this region is highly complex. Its tidal phase stays almost constant between ~ 100 and 110 km, a feature of the “evanescent” wave that is, absent in both the model predictions and TIMED/SABER observations. The newly observed tidal modulation is almost out of phase with the established results in the turbopause region. Its zig-zag phase profile below 98 km is consistent with early established climatological results.

The capability of day and night observation of the USU Na lidar in the MLT above mid-latitudes, also provides a unique opportunity to validate the new MIGHTI/ICON measurements. This investigation has demonstrated good agreement on temperature measurements in the summertime between the two instruments within the overlapping altitude range (~ 90 – 104 km during the night and ~ 90 – 98 km during the day) with the differences less than the measurement uncertainties. This allows us to conduct more future investigations on the dynamics in the turbopause region.

Appendix: Daytime Temperature Validation

During the March campaign 2021, the USU Na lidar changed the system set up to conduct collaborative day and night temperature observations with MIGHTI/ICON. The lidar operated 15 days, 160 h (82 h in the daytime), providing a considerable amount of overlap observations with the MIGHTI/ICON. Figure A illustrates the average temperature profiles of four afternoon hours (LST 14:00–17:00) based on the lidar and MIGHTI/ICON observations during this period. The data are processed the same way as we presented in this paper. Note that the lidar measurements during this campaign reached ~ 100 km, higher than the upper limit during the summer months. These new data demonstrate good agreement on the daytime temperature observations between the two instruments. The differences are within the uncertainty of the measurements, as we stated in the manuscript. We also compared all the temperature measurements by MIGHTI and the lidar within the overlapping altitude range (~ 90 – 100 km) and calculated the Pearson correlation coefficients of the two temperature series, indicating high correlation (e.g., $R = 0.80$ at 93 km and $R = 0.82$ at 96 km, respectively). The outlier in the right plot in Figure A1, which the MIGHTI has a much higher temperature than the lidar measured (~ 210 vs. 168 K), occurred near 99 km for LST 10:00 when the MIGHTI only had 2 sampling profiles during the course of the campaign.

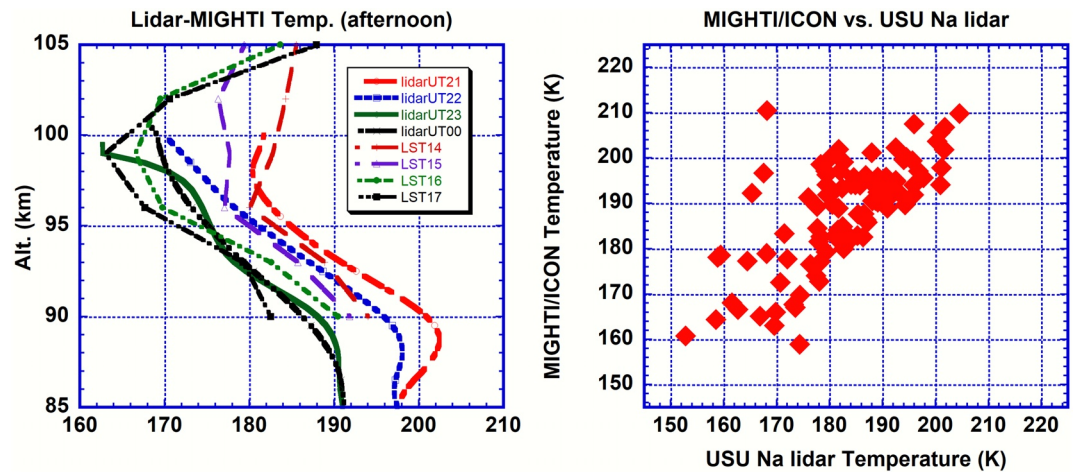


Figure A1. The comparisons of daytime temperature profiles between the USU Na lidar and MIGHTI/ICON during the March Campaign 2021 for four afternoon hours between LST 14:00 and LST 17:00 (UT 21:00 and UT 24:00; left). The pair of hourly averaged profiles with the same color represent the observations during the same hour. The relationship between the MIGHTI/ICON and the lidar temperatures (right) within the overlapping range of $\sim 90\text{--}99$ km altitude.

Data Availability Statement

The lidar data of this study are available through “USU Na lidar Data” (<https://doi.org/10.15142/T33H26>, Yuan, 2018). The MIGHTI/ICON data can be downloaded at https://pdf.gsfc.nasa.gov/pub/data/icon/12/12-3_mighti-a_temperature/2020/ and https://pdf.gsfc.nasa.gov/pub/data/icon/12/12-3_mighti-b_temperature/2020/. The CTMT results can be accessed at <https://globaldynamics.sites.clemson.edu/articles/ctmt.html>.

Acknowledgments

The USU Na lidar is supported by National Science Foundation grant number AGS1954308 and AGS 2125712. ICON is supported by NASA’s Explorers Program through contracts NNG-12FA45C and NNG12FA42I. We also want to thank Dr. V. Wickwar for making the Rayleigh lidar receiving mirrors accessible to the Na lidar operations.

References

- Baumgarten, K., & Stober, G. (2019). On the evaluation of the phase relation between temperature and wind tides based on ground-based measurements and reanalysis data in the middle atmosphere. *Annals of Geophysics*, 37, 581–602. <https://doi.org/10.5194/angeo-37-581-2019>
- Becker, E. (2017). Mean-flow effects of thermal tides in the mesosphere and lower thermosphere. *Journal of the Atmospheric Sciences*, 74(6), 2043–2063. <https://doi.org/10.1175/jas-d-16-0194.1>
- Cai, X., Yuan, T., & Eccles, J. V. (2017). A numerical investigation on tidal and gravity wave contributions to the summer time Na variations in the midlatitude E region. *Journal of Geophysical Research: Space Physics*, 122(10), 10577–10595. <https://doi.org/10.1002/2016JA023764>
- Cai, X., Yuan, T., Zhao, Y., Pautet, P.-D., Taylor, M. J., & Pendleton, W. R., Jr. (2014). A coordinated investigation of the gravity wave breaking and the associated dynamical instability by a Na lidar and an Advanced Mesosphere Temperature Mapper over Logan, UT (41.7N, 111.8W). *Journal of Geophysical Research: Space Physics*, 119, 6852–6864. <https://doi.org/10.1002/2014JA020131>
- Carter, L. N. and Forbes, J. M. (1999): Global transport and localized layering of metallic ions in the upper atmosphere, *Annals of Geophysics*, 17, 190–209. <https://doi.org/10.1007/s00585-999-0190-6>
- Dhadly, M. S., Emmert, J. T., Drob, D. P., McCormack, J. P., & Niciejewski, R. (2018). Short-term and interannual variations of migrating diurnal and semidiurnal tides in the mesosphere and lower thermosphere. *Journal of Geophysical Research: Space Physics*, 123, 7106–7123. <https://doi.org/10.1029/2018JA025748>
- Englert, C. R., Harlander, J. M., Brown, C. M., Marr, K. D., Miller, I., Stump, J. E., et al. (2017). Michelson interferometer for global high-resolution thermospheric imaging (MIGHTI): Instrument design and calibration. *Reviews of Space Science*, 212, 553–584. <https://doi.org/10.1007/s11214-017-0358-4>
- Forbes, J. M. (1995). Tidal and planetary waves. In R. M. Johnson, & T. L. Killeen (Eds.), *The upper mesosphere and lower thermosphere: A review of experiment and theory* (pp. 67–87). <https://doi.org/10.1029/GM087p0067>
- Forbes, J. M., & Garrett, H. B. (1979). Theoretical studies of atmospheric tides. *Reviews of Geophysics and Space Physics*, 17, 1951–1981. <https://doi.org/10.1029/rg017i008p01951>
- Forbes, J. M., & Hagan, M. E. (1988). Diurnal propagating tide in the presence of mean winds and dissipation: A numerical investigation. *Planetary and Space Science*, 36(6), 579–590. [https://doi.org/10.1016/0032-0633\(88\)90027-x](https://doi.org/10.1016/0032-0633(88)90027-x)
- Forbes, J. M., Zhang, X., Hagan, M. E., England, S. L., Liu, G., & Gasperini, F. (2017). On the Specification of upward-propagating tides for ICON science investigations. *Space Science Reviews*, 212, 697–713. <https://doi.org/10.1007/s11214-017-0401-5>
- Forbes, J. M., Zhang, X., Palo, S., Russell, J., Mertens, C. J., & Mlynarczyk, M. (2008). Tidal variability in the ionospheric dynamo region. *Journal of Geophysical Research*, 113, A02310. <https://doi.org/10.1029/2007JA012737>
- Hagan, M. E., & Forbes, J. M. (2002). Migrating and nonmigrating diurnal tides in the middle and upper atmosphere excited by tropospheric latent heat release. *Journal of Geophysical Research*, 107(D24), 4754. <https://doi.org/10.1029/2001JD001236>

- Hagan, M. E., & Forbes, J. M. (2003). Migrating and nonmigrating semidiurnal tides in the upper atmosphere excited by tropospheric latent heat release. *Journal of Geophysical Research*, *108*(A2), 1062. <https://doi.org/10.1029/2002JA009466>
- Hines, C. O. (1997a). Doppler-spread parameterization of gravity wave momentum deposition in the middle atmosphere. Part 1: Basic formulation. *Journal of Atmospheric and Solar-Terrestrial Physics*, *59*, 371–386. [https://doi.org/10.1016/s1364-6826\(96\)00079-x](https://doi.org/10.1016/s1364-6826(96)00079-x)
- Hines, C. O. (1997b). Doppler-spread parameterization of gravity wave momentum deposition in the middle atmosphere. Part 2: Broad and quasi monochromatic spectra, and implementation. *Journal of Atmospheric and Solar-Terrestrial Physics*, *59*, 387–400. [https://doi.org/10.1016/s1364-6826\(96\)00080-6](https://doi.org/10.1016/s1364-6826(96)00080-6)
- Immel, T. J., England, S. L., Mende, S. B., Heelis, R. A., Englert, C. R., Edelstein, J., et al. (2018). The Ionospheric connection explorer mission: Mission goals and design. *Space Science Reviews*, *214*, 13. <https://doi.org/10.1007/s11214-017-0449-2>
- Krueger, D. A., She, C.-Y., & Yuan, T. (2015). Retrieving mesopause temperature and line-of-sight wind from full-diurnal-cycle Na lidar observations. *Applied Optics*, *54*, 9469–9489. <https://doi.org/10.1364/ao.54.009469>
- Liu, H.-L., & Hagan, M. E. (1998). Local heating/cooling of the mesosphere due to gravity wave and tidal coupling. *Geophysical Research Letters*, *25*, 2941–2944. <https://doi.org/10.1029/98gl02153>
- McLandress, C. (2002). The seasonal variation of the propagating diurnal tide in the mesosphere and lower thermosphere. Part II: The role of tidal heating and zonal mean winds. *Journal of the Atmospheric Sciences*, *59*, 907–922. [https://doi.org/10.1175/1520-0469\(2002\)059<0907:tsvotp>2.0.co;2](https://doi.org/10.1175/1520-0469(2002)059<0907:tsvotp>2.0.co;2)
- Oberheide, J., & Forbes, J. M. (2008). Tidal propagation of deep tropical cloud signatures into the thermosphere from TIMED observations. *Geophysical Research Letters*, *35*, L04816. <https://doi.org/10.1029/2007GL032397>
- Oberheide, J., Forbes, J. M., Zhang, X., & Bruinsma, S. L. (2011). Climatology of upward propagating diurnal and semidiurnal tides in the thermosphere. *Journal of Geophysical Research*, *116*, A11306. <https://doi.org/10.1029/2011JA016784>
- Ortland, D. A., & Alexander, M. J. (2006). Gravity wave influence on the global structure of the diurnal tide in the mesosphere and lower thermosphere. *Journal of Geophysical Research*, *111*, A10S10. <https://doi.org/10.1029/2005JA011467>
- Roeckner, E., Brokopf, R., Esch, M., Giorgetta, M., Hagemann, S., Kornblueh, L., et al. (2006). Sensitivity of simulated climate to horizontal and vertical resolution in the ECHAM5 atmosphere model. *Journal of Climate*, *19*, 3771–3791. <https://doi.org/10.1175/jcli3824.1>
- Schmidt, H., Brasseur, G. P., Charron, M., Manzini, E., Giorgetta, M. A., Diehl, T., et al. (2006). The HAMMONIA chemistry climate model: Sensitivity of the mesopause region to the 11-year solar cycle and CO₂ doubling. *Journal of Climate*, *19*, 3903–3931. <https://doi.org/10.1175/jcli3829.1>
- She, C.-Y., Krueger, D. A., Yuan, T., & Oberheide, J. (2016). On the polarization relations of diurnal and semidiurnal tide in the mesopause region. *Journal of Atmospheric and Solar-Terrestrial Physics*, *142*, 60–71. <https://doi.org/10.1016/j.jastp.2016.02.024>
- She, C.-Y., Li, T., Collins, R. L., Yuan, Williams, B. P., Kawahara, T., & et al. (2004). Tidal perturbations and variability in mesopause region over Fort Collins, CO (41°N, 105°W): Continuous multi-day temperature and wind lidar observations. *Geophysical Research Letters*, *31*(24). <https://doi.org/10.1029/2004gl021165>
- Stevens, M. H., Englert, C. R., Harlander, J. M., England, S. L., Marr, K. D., Brown, C. M., & Immel, T. J. (2018). Retrieval of lower thermospheric temperatures from O₂ A band emission: The MIGHTI experiment on ICON. *Space Science Reviews*, *214*, 4. <https://doi.org/10.1007/s11214-017-0434-9>
- Yuan, T. (2018). *USU Na lidar data*. Utah State University. <https://doi.org/10.15142/T33H26>
- Yuan, T., Schmidt, H., She, C. Y., Krueger, D. A., & Reising, S. (2008a). Seasonal variations of semidiurnal tidal perturbations in mesopause region temperature and zonal and meridional winds above Fort Collins, Colorado (40.6°N, 105.1°W). *Journal of Geophysical Research*, *113*, D20103. <https://doi.org/10.1029/2007JD009687>
- Yuan, T., She, C. Y., Forbes, J., Zhang, X., Krueger, D., & Reising, S. (2010). A collaborative study on temperature diurnal tide in the mid-latitude mesopause region (41°N, 105°W) with Na lidar and TIMED/SABER observations. *Journal of Atmospheric and Solar-Terrestrial Physics*, *72*, 541–549. <https://doi.org/10.1016/j.jastp.2010.06.012>
- Yuan, T., She, C. Y., Hagan, M. E., Williams, B. P., Li, T., Arnold, K., et al. (2006). Seasonal variation of diurnal perturbations in mesopause region temperature, zonal, and meridional winds above Fort Collins, Colorado (40.6°N, 105°W). *Journal of Geophysical Research*, *111*, D06103. <https://doi.org/10.1029/2004JD005486>
- Yuan, T., She, C. Y., Kawahara, T. D., & Krueger, D. A. (2012). Seasonal variations of mid-latitude mesospheric Na layer and its tidal period perturbations based on full-diurnal-cycle Na lidar observations of 2002–2008. *Journal of Geophysical Research*, *117*, D11304. <https://doi.org/10.1029/2011jd017031>
- Yuan, T., She, C. Y., Krueger, D. A., Sassi, F., Garcia, R., Roble, R. G., et al. (2008b). Climatology of mesopause region temperature, zonal wind, and meridional wind over Fort Collins, Colorado (41°N, 105°W), and comparison with model simulations. *Journal of Geophysical Research*, *113*, D03105. <https://doi.org/10.1029/2007JD008697>
- Yuan, T., She, C. Y., Oberheide, J., & Krueger, D. A. (2014). Vertical tidal wind climatology from full-diurnal-cycle temperature and Na density lidar observations at Ft. Collins, CO (41°N, 105°W). *Journal of Geophysical Research–D: Atmospheres*, *119*, 4600–4615. <https://doi.org/10.1002/2013JD020338>
- Yuan, T., Solomon, S. C., She, C.-Y., Krueger, D. A., & Liu, H.-L. (2019). The long-term trends of nocturnal mesopause temperature and altitude revealed by Na lidar observations between 1990 and 2018 at midlatitude. *Journal of Geophysical Research–D: Atmospheres*, *124*, 5970–5980. <https://doi.org/10.1029/2018JD029828>
- Zhang, X., Forbes, J. M., Hagan, M. E., Russell, J. M., III, Palo, S. E., Mertens, C. J., & Mlynczak, M. G. (2006). Monthly tidal temperatures 20–120 km from TIMED/SABER. *Journal of Geophysical Research*, *111*, A10S08. <https://doi.org/10.1029/2005JA011504>